

# Boundary Layer Water Vapor Variations at the Southern Great Plains Site Derived from Multiyear Raman Lidar Measurements

*K. Taniguchi and Z. Wang  
Department of Atmospheric Science  
University of Wyoming  
Laramie, Wyoming*

## Introduction

Lately, climate change has become a major concern for our society. However, it is not easy to understand the climate entirely as it is the accumulative result of the earth system (both anthropogenic and natural effects). As awareness of the complexity of the earth system increases, the study of climate needs to involve the modeling of the entire planetary system. Modeling would benefit from improvement in the knowledge of any physical process. In particular, water vapor has a great potential for advancing models because of its extended effects in various aspects. As a part of the hydrological cycle, water vapor is clearly associated with the evolution of cloud and precipitation. The evolution not only impacts the biosphere and human activities, but also affects the heat balance of the earth because of water vapor's effective role in the transporter of heat. Also, water vapor influences the radiation balance of the atmosphere directly and indirectly; water vapor is a powerful greenhouse gas, while clouds reduce incoming solar radiation and outgoing terrestrial radiation. Furthermore, water vapor contributes to several chemical processes. While evaporation helps in releasing some particles into the atmosphere, precipitation transports chemical components from the atmosphere to the earth surfaces. The presence of water vapor in the atmosphere promotes certain chemical reactions and delays others. Thus, the study of water vapor behavior in the atmosphere will help us better understand climate and earth system in numerous applications.

Unfortunately, the inhomogeneous horizontal and vertical distribution of water vapor makes related effects heterogeneous and complicated to estimate. To acquire better knowledge of water vapor distributions on different temporal and spatial scales, various measurement methods have been employed.

Since Melfi et al. (1969) and Cooney (1968) introduced it in the late 1960's, the Raman lidar has become a well-established method for water vapor observation (Whiteman et al. 1992). In addition to its simple concept, the Raman lidar has some advantages over other instruments. Global positioning system (GPS)-based measurements derive the total water vapor from measured signal delays along the

signal's paths. With its great accessibility, GPS has the potential to achieve fine resolutions and capture some of the water vapor variation (Bengtsson et al. 2003). Although coarsely resolved vertical water vapor measurements are available at a few locations, the GPS data obtained is normally the total precipitable water vapor. The traditional two-channel microwave radiometer can also only provide vertically integrated precipitable water vapor. Unlike GPS or microwave radiometer measurements, the Raman lidar provides vertically resolved water vapor observations. The continuous measurement ability of the Raman lidar also allows for fine temporal resolution. Although radiosondes provide valuable observations of water vapor and other atmospheric properties, the temporal and spatial resolution of such in situ measurements are too coarse for water vapor variation characterization. Hence, the Raman lidar supplies the best measurements for studying temporal and spatial variations of water vapor.

As a part of the Atmospheric Radiation Measurement (ARM) program, Raman lidar has been operated at the Southern Great Plane (SGP) site Cloud and Radiation Testbed facility in Northern Oklahoma for ~10 years. The ARM program has an objective of obtaining accurate and continuous long-term water vapor and cloud measurements to enhance our knowledge of radiation transfer processes (<http://www.arm.gov/>; Goldsmith et al. 1998). To examine the boundary layer water vapor variations, Raman lidar data obtained over 5 years at the SGP site are employed. Inconsistent incoming solar radiation is known to introduce diurnal and seasonal variations. Thus, this study will present water vapor behavior characteristics based on studies of diurnal and seasonal variation in temporal and vertical spaces.

## Instruments and Data

The Cloud and Radiation Testbed Raman lidar transmits a third harmonic Nd:YAG laser (355 nm, 400 mJ energy/pulse) vertically with a repetition rate of 30Hz. The laser beam is expanded to 13 cm in diameter for eye-safety. A 61-cm-diameter receiver collects Raman signals at wavelengths centered at 387 nm, 408 nm and 355 nm from nitrogen, water vapor and aerosol, respectively. The water vapor mixing ratio – i.e., the mass ratio of water vapor and dry air within a given volume – can be derived from the Raman signals for water vapor and nitrogen. The ARM Raman lidar data is available as calibrated profiles of water vapor mixing ratio together with the associated random error estimation. Normally, the data obtained is within an uncertainty of 5% and detection limit of 0.002 g/kg (Turner et al. 2002; Whiteman et al. 2006). For the technical and data processing details of the Raman lidar system at the SGP site, please refer to the literature (Goldsmith et al. 1998; Bisson et al. 1999; Turner and Goldsmith 1999; and Turner et al. 2002). Although the range of the Raman lidar can be extended farther, this study focuses on the lowest 2 km of the atmospheric layer where most of the water vapor is concentrated.

The Raman lidar data analyzed in this study was obtained at the SGP site almost continuously between March 1998 and August 2003. Because of the calibration routine, as well as the mechanical and environmental conditions, the Raman lidar data quality varies. To ensure the quality of the study,

screening processes were applied to the whole dataset. First, data used for analysis must contain no more than 1-hour break within the calculation periods ( $\Delta t$ ). Second, only data with estimated random error less than 15% are used for analysis, which minimizes the potential noise impact on the results. The number of days that satisfied the screening requirements is presented in Table 1. The data was grouped into the following four seasons: spring (March, April, May), summer (June, July, August), fall (September, October, November) and winter (December, January, February). Unfortunately, the Raman lidar has problems under rainy, low-level cloud and foggy conditions (Wechwerth et al. 1999). Under such conditions, the observation may contain severe noise. Thus, data under rainy or foggy conditions were excluded in the present study. Although the presence of mid- and high-level clouds reduces the observation range to some degree, its effects are expected to be insignificant in the lowest 2 km layer. Hence, the selected data still represents conditions under both clear and cloudy sky.

Month	Mar	Apr	May	June	July	Aug	Sep	Oct	Nov	Dec	Jan	Feb
Days	64	85	69	68	51	63	68	62	61	72	45	10
Season	Spring			Summer			Fall			Winter		
Days	218			182			191			127		

## Methodology and Results

For each day, sunrise, noon, sunset, and midnight times (these will be referred as solar events hereafter) were calculated based on the geographical coordinates of the SGP site and the time of the year. In this study, noon (tnoon) and midnight (tnight) refer to the mid-time between sunrise (trise1) and sunset (tset), and between tset and sunrise of next day (trise2) as shown in Figure 1. For convenience, a day in this study starts 4 hours before sunrise time and ends 2 hours after midnight, rather than Universal Time Coordinates or local time. Multifilter rotating shadowband radiometer data collected at the SGP site was used to verify the accuracy of the solar time calculations.

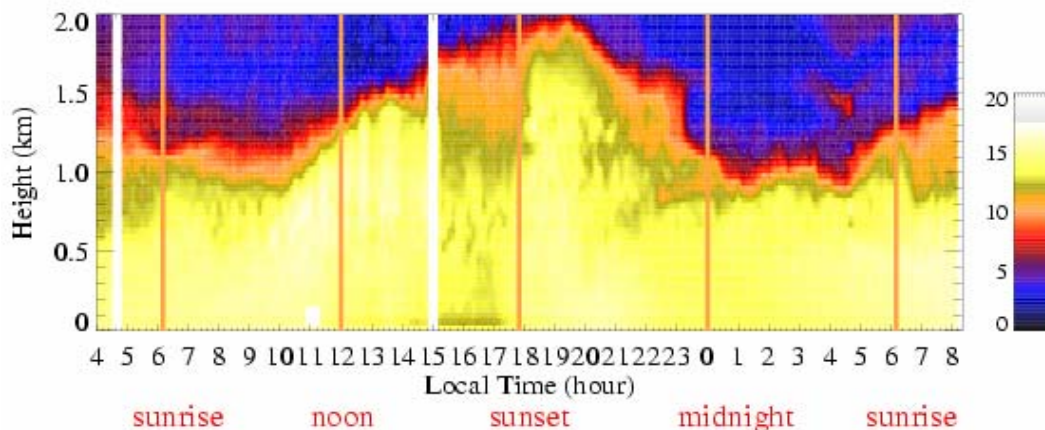


**Figure 1.** Water vapor mixing ratio (g/kg) observed by Raman lidar at the SGP site on 25 September 1998. The narrow orange lines indicate calculated solar event times.

The mean and standard deviation of water vapor mixing ratio over periods from 10 minutes to 4 hours were calculated 5 times a day, arranged around the solar events. The starting and ending times of the calculations are summarized in Table 2. The daily means and standard deviations were used to generate monthly and seasonal statistics. Because each month contains a different number of selected days as shown in Table 1, the seasonal averages were weighted by day rather than by month. All standard deviations were normalized by the corresponding means.

**Table 2.** The starting and ending time of mean and standard deviation calculations for each solar event.

Solar Event	Starting Time	Ending Time
Before Sunrise	Trisel - $\Delta t$	Trisel
After Sunrise	Trisel	trisel + $\Delta t$
Noon	tnoon - $0.5\Delta t$	tnoon + $0.5\Delta t$
Sunset	tset - $\Delta t$	tset
Midnight	tnight - $0.5\Delta t$	tnight + $0.5\Delta t$
Note: $\Delta t$ represents the length of the calculation period. It ranges between 10min and 4hrs.		

To examine the temporal variation of the water vapor mixing ratio, Figure 2 shows the normalized standard deviation as a function of the calculation period length ( $\Delta t$ ), from 10 minutes to 4 hours. For each period  $\Delta t$ , the normalized standard deviation represents the standard deviations averaged over a 2 km-layer. Regardless of the season or time of the day, the variation increases with the length of  $\Delta t$ . The winter variation shows an especially rapid growth as  $\Delta t$  increases. The summer variation is the least sensitive to changes in  $\Delta t$ . In fact, winter variation over a 1-hour period is as high as summer variation over a 3-hour period. The largest seasonal differences appear around sunrise, while seasonal stability appears around noon. Unlike the seasonal relative differences, the diurnal relative difference is reduced with increasing  $\Delta t$ . Remarkably, the temporal variation of the water vapor mixing ratio in spring shows a close resemblance to the summer, and similarly the fall to winter.

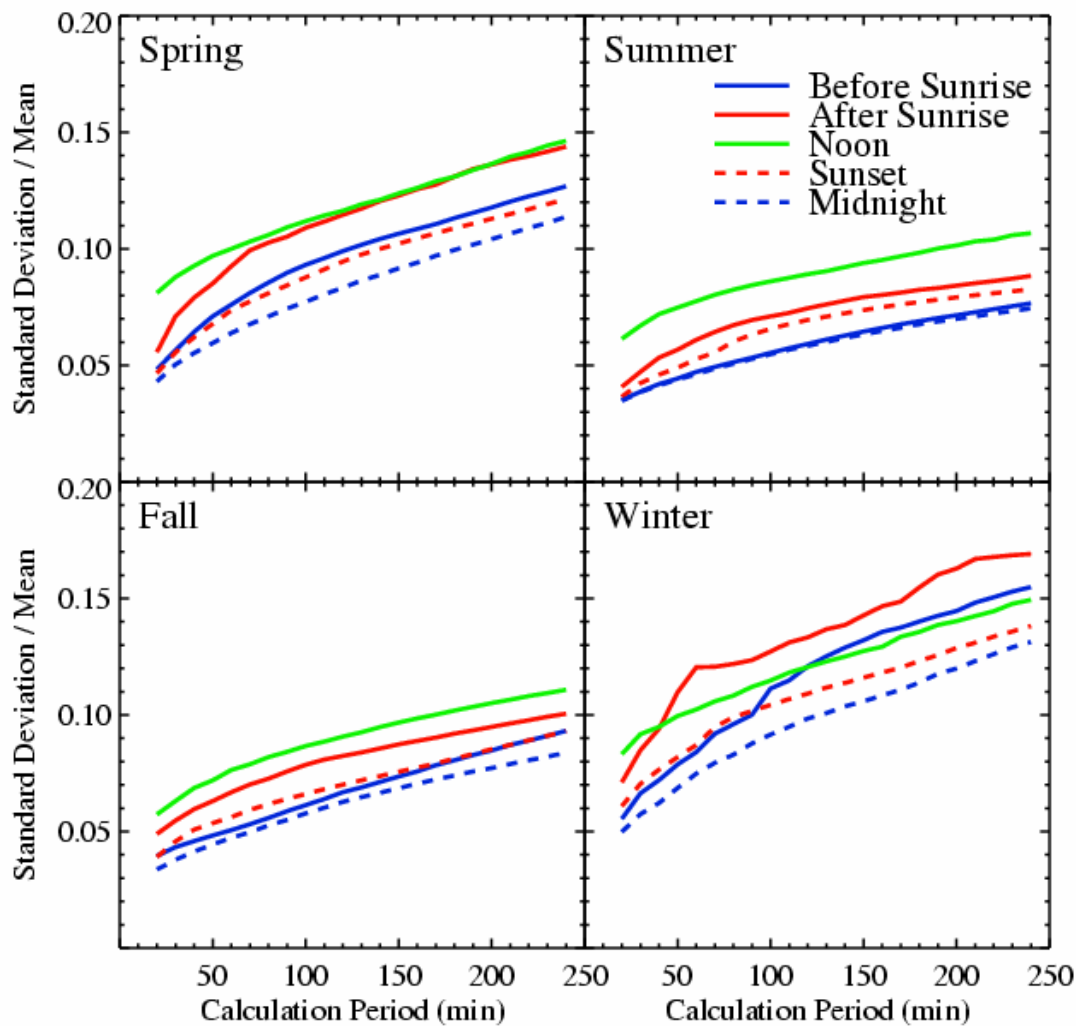


**Figure 2.** The average temporal variation of water vapor mixing ratio within the lowest 2 km boundary layer as a function of  $\Delta t$  for four seasons.

The relationship between the mean water vapor mixing ratio and height shows great seasonal differences. However, the strong temperature dependency of the water vapor saturation mixing ratio prevents better characterizations of the vertical variation of water vapor mixing ratio without continuous temperature profiles. Therefore, the vertical dependency of mean water vapor mixing ratio is not studied here. To study the vertical dependency of the water vapor mixing ratio variation, the normalized standard deviation as a function of height is illustrated in Figure 3. The seasonal dependency of the vertical trends can be observed clearly. The winter profile indicates maximum relative variations, whereas the summer profile shows a minimum. At a 1-km altitude, the relative variation in winter is roughly 50% greater than that of the summer. The increasing in normalized standard deviation with height is largest in winter and the smallest in summer. These seasonal differences are more pronounced around noon for most altitudes. The seasonal and diurnal differences seem to be affected by the boundary layer mixing, so a detailed study will be performed in the future.

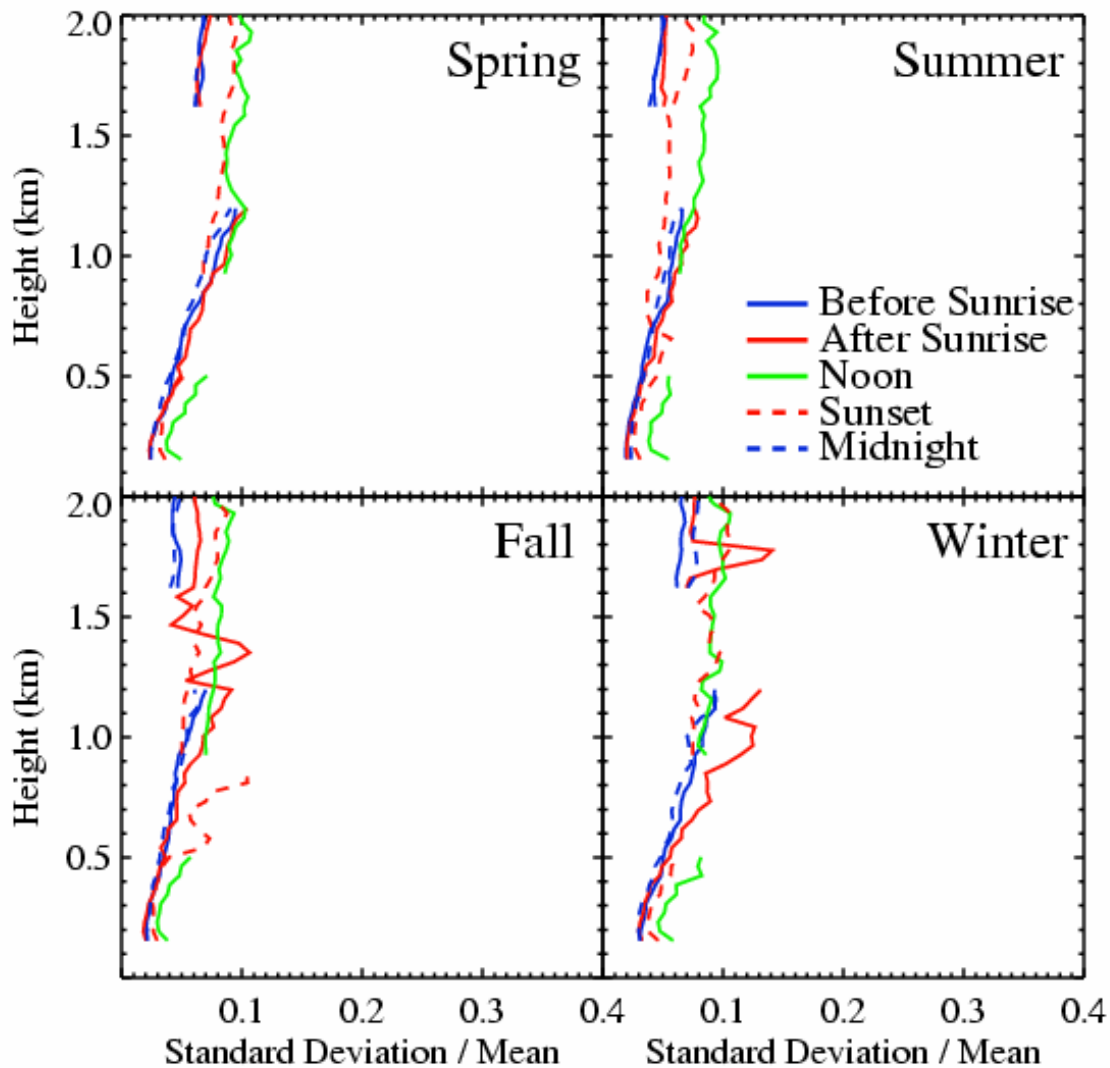


**Figure 3.** The vertical dependency of normalized standard deviations of water vapor mixing ratio over 1-hour periods for four seasons.

In Figure 3, the profiles show blanks at heights between 1.2 km and 1.6 km for the sunrise and midnight profiles, and between 0.6 km and 0.9 km for the noon profiles. In the Cloud and Radiation Testbed Raman lidar, a dual field of view receiving system is employed to improve the observation range. However, the system introduces severe error for the region around the transitional altitude. As a result, profiles have discontinuities due to high random error data, which was excluded in the screening process as discussed in the Instruments and Data section. Since disconnected profiles are not aligned, a simple linear modification is not the best solution. We will explore new approaches to optimally merge the dual view water vapor measurements to better characterize the vertical dependencies of water vapor variations.

## Summary

Over 5 years of Raman lidar data acquired at the SGP-site Cloud and Radiation Testbed facility as a part of the ARM program was used in order to study water vapor inhomogeneity in the boundary layer. To ensure reliable results, screening processes were performed to the data, which reduced the total number of days down to 718. Within the 2 km layer of the lowest atmosphere, means and standard deviations over various periods ( $10 \text{ min} \leq \Delta t \leq 4 \text{ hr}$ ) were calculated 5 times a day based on the calculated solar event times. To assess the seasonal impacts on the water vapor variation, seasonal values were derived from daily results.

For temporal variations, 2 km-average normalized standard deviations were plotted as a function of  $\Delta t$ . Winter shows the largest variation, whereas summer indicates the least. Seasonal differences appear most around sunrise. However, the seasonal relative variations increase as  $\Delta t$  increases, whereas the diurnal relative variations decrease with increasing  $\Delta t$ . Similarities can be observed between spring and summer, as well as between fall and winter, especially around noon.

Also, the vertical dependency of temporal variation was seasonally analyzed. Although the profiles contain discontinuities due to the high random error at transitional altitudes of the dual field of view, the profiles provide an overview of the vertical dependency of the seasonal water vapor variation. In general, the variation increases with height, and the increasing rates are seasonally influenced. Rapid changes with height are observed in winter and gradual changes are observed in summer. Therefore, seasonal differences at solar events are enhanced at higher altitudes. The water vapor variation is mainly controlled by seasonal cycles and to a lesser extent by diurnal cycles. The boundary layer mixing seems to have an important role in the seasonal and diurnal differences.

For further research, a new methods of merging the data from the dual field system needs to be investigated to remove the discrepancy. Based on the new method results, the relationship between the water vapor mixing ratio variation and the mixing of the boundary layer will be analyzed in detail. Also, the vertical water vapor mixing ratio variations will be performed with adequate temperature profiles. To better understand the water vapor variations, meteorological and other observations around the SGP site will be used for the analysis.

## Acknowledgments

Data were obtained from the ARM Program sponsored by the U.S. Department of Energy, Office of Science, Office of Biological and Environmental Research, Environmental Sciences Division.

## Contact

Kyoko Taniguchi  
[Kyoko76@uwyo.edu](mailto:Kyoko76@uwyo.edu)  
Department of Atmospheric Science  
University of Wyoming  
Laramie WY 82071

## References

- Bengtsson, L, G Robinson, R Anthes, K Aonashi, A Dodson, G Elgered, G Gendt, R Gurney, M Jietai, C Mitchell, M Mlaki, G Rhodin, P Silverstrin, R Ware, R Watson, and W Wrgen. 2003. "The use of GPS measurements for water vapor determination." *American Meteorological Society* 84:1249-1258.
- Bisson, SE, JEM Goldsmith, and MG Michell. 1999. "Narrow-band, narrow-field-of-view the Raman lidar with combined day and night capability for tropospheric water-vapor profile measurements." *Applied Optics* 38:1841-1849.
- Cooney, JA. 1968. "Measurements on the Raman component of laser atmospheric backscatter." *Applied Physics Letters* 12:40-42.
- Goldsmith, JEM, FH Blair, SE Bisson, and DD Turner. 1998. "Turn-key the Raman lidar for profiling atmospheric water vapor, clouds, and aerosols." *Applied Optics* 37:4979-4989.
- Melfi, SH, JD Lawrence, and MP McCormick. 1969. "Observation of the Raman scattering by water vapor in the atmosphere." *Applied Physical Letters* 15:295-297.
- Turner, DD, and JEM Goldsmith. 1999. "Twenty-four-hour the Raman lidar water vapor measurements during the Atmospheric Radiation Measurement Program's 1996 and 1997 water vapor intensive observation periods." *Journal of Atmospheric Oceanic Technology* 16:1062-1076.
- Turner, DD, RA Ferrare, LA Heilman, WF Feltz, and TP Tooman. 2002. "Automated retrievals of water vapor and aerosol profiles from an operational the Raman lidar." *Journal of Atmospheric and Oceanic Technology* 19:37-50.
- Wechwerth, TM, V Wulfmeyer, RM Wakimoto, RM Hardesty, JW Wilson, and RM Banta. 1999. "NCAR-NOAA lower-tropospheric water vapor workshop." *Bulletin of the American Meteorological Society* 80:2339-2357.

Whiteman, DN, SH Melfi, and RA Ferrare. 1992. The Raman lidar system for measurement of water vapor and aerosols in the Earth's atmosphere." *Applied Optics* 31:3068-3082.

Whiteman, DN, F Russo, B Demoz, LM Miloshevich, I Veselovskii, S Hannon, Z Wang, H Vömel, F Schmidlin, B Lesht, PJ Moore, AS Beebe, A Gambacorta, and C Barnet. 2006. "Analysis of the Raman lidar and radiosonde measurements from the AWEX-G field campaign and its relation to Aqua validation." *Journal of Geophysical Research* (in press).